Modeling the Mechanical Properties of Pulmonary Alveoli with Fibrosis and Other Lung Diseases

Laura R. Caggiano[1]

[1]Department of Biomedical Engineering, Ohio State University, Columbus, OH 43210

Honors Thesis

Presented in the Partial Fulfillment of the Requirements for the Degree Bachelor of Science in Biomedical Engineering with Honors Research Distinction of The Ohio State University

The Ohio State University

2014

Defense Committee:

Dr. Samir Ghadiali, Advisor

Dr. Thomas Hund

Abstract

Idiopathic pulmonary fibrosis (IPF) is the most common interstitial lung disease in the world. Of all interstitial pneumonias, it also has the most unfavorable prognosis and is considered more deadly than several cancers. IPF also has no known treatments or therapies to effectively combat the disease. There is no current way to measure the local mechanical deformations of fibrotic alveolar geometries *in vivo.* The resolution of current imaging modalities is too poor to capture the complex microstructure of lung tissue non-invasively. Therefore, to develop efficacious treatments for this disease, it has become very important to be able to accurately reproduce the damage caused by fibrosis in a lab setting. A new method of computationally simulating the mechanical properties of diseased lung tissue has been developed using microscopic images of histological slides containing fibrotic and healthy mouse lung tissue. This method uses software including ImageJ, COMSOL, and MATLAB to process these images and simulate their mechanical response to a biaxial tensile test under physiologically appropriate boundary conditions. This method was used to process several microscopic images taken at different time points throughout the progression of the disease. Results using this method indicate significant deformation as well as changes in maximum strain values throughout the tissue samples. This data will be used to produce a device that will reproduce the mechanical behavior of fibrotic lung tissue, commonly referred to as “lab-on-a-chip” technology. This device will allow pulmonary researchers to better predict the outcomes of treatments for IPF to improve patients' quality of life and ultimately find a cure.

Acknowledgements

This work is supported by an undergraduate honors thesis scholarship from The Ohio State University College of Engineering to LRC. The authors would like to thank the Campus Microscopy & Imaging Facility at the Wexner Medical Center for the use of their multiphoton microscope, as well as Dr. Michael Ostrowski for providing the transgenic tissue samples used in this study.

Table of Contents

List of Tables

List of Figures

1 Introduction

IPF is a both a progressive lung disease of unknown cause characterized by scar tissue accumulation in the lungs and a devastating prognosis. Individuals with IPF are typically between the ages of 40 and 70 years old, and live a median of only 2.5-3.5 years after diagnosis. The five-year survival rate for patients with IPF is 20%, which is lower than that of patients with pulmonary adenocarcinoma [1]. The incidence of IPF in the United States is estimated to be 16.3 per 100,000, making it the most common interstitial lung disease in the world [2]. Because it is a cryptogenic disease, there is currently no cure for IPF; the only treatments that exist serve to slow its progression and improve patients' quality of life [3,4].

While the pathology of IPF is not entirely understood, prevailing hypotheses state that it originates with repeated epithelial injury, spurring the activation of alveolar epithelial cells (AECs). AECs activate the proliferation of fibroblasts and myofibroblasts, which synthesize and lay down extracellular matrix (ECM). The damaged basement membrane of the original lung tissue prohibits re-epithelialization and the epithelial to mesenchymal transition (EMT) from proceeding properly. This results in an excessive accumulation of scar tissue over time due to the continued presence of fibroblasts [5]. Fibroblasts are known to be responsive to the mechanical forces from the environment in which they reside. Studies have shown that ECM is laid down differently under varying environmental forces [6]. Since fibroblasts play a role in the development of IPF, characterizing the mechanical properties of lung tissue has become one of the main focus points of understanding the pathogenesis of the disease [5].

Several studies have sought to investigate lung tissue mechanics, which are highly complex and dynamic. Even for healthy lungs, the tortuous geometry and surface tension in addition to the stiffening of parenchymal tissue present a challenge in that their nonlinearity is

difficult to characterize with any singular equation or model [7]. This problem is exacerbated by the fact that it is nearly impossible to image alveolar geometries *in vivo* and non-invasively. Currently, the preferred method for imaging lungs is through X-ray computed tomography (CT) [8]. However, the resolution of CT is too poor to capture the complex microstructure of alveolar tissue. As a result, recent efforts have been made to examine the mechanical properties of lung tissue *in vitro*. In 2010, a microfluidic device was developed that reproduced organ-level functions of the human alveolar-capillary interface. The lung-on-a-chip device consists of a poly(dimethylsiloxane) (PDMS) membrane coated with ECM, and simulates the mechanical stretching of physiological breathing by applying a vacuum to two side chambers [9]. This microdevice has largely expanded the capabilities of cell culture models to be used for toxicology and therapeutic applications by providing a low-cost substitute for human and animal studies. Since the development of biomimetic system, several more studies have sought to employ its design to investigate various lung disorders such as drug toxicity-induced edema, acute lung injury, and emphysema [10,11].

To further advance the goal of understanding the pathology of IPF, investigators have begun to apply different parameters of the alveolar environment to this micro-nanoscale system such as fiber stiffness and geometry with the goal of being able to mimic IPF in an *in vitro* model [10]. While these models have been able to reproduce several environmental factors such as fluid flow and surface tension, they fall short in their ability to replicate how lung tissue responds to mechanical loads such as stretching and positive pressures. These mechanical aspects of lung tissue play a part in many pulmonary processes including cell proliferation, ECM modeling, wound healing, and apoptosis. Therefore, it is crucial that they be represented accurately in an *in vitro* model. To make progress toward the goal of replicating the mechanical properties of

fibrotic lung tissue in a biomimetic microsystem, this study aims to investigate those properties *in silico* by simulating the effect environmental forces on healthy and fibrotic lung tissue in mice.

Previous studies indicate that phosphorylated ets-2 plays an important role in ECM remodeling and lung inflammation [12]. With this information, the models of lung tissue were created using two separate strains of mice. Ets-2 (A72/A72) transgenic mice (containing a mutated version of ets-2 at site threonine-72) were used for the normal tissue model, and ets-2 (wild-type/wild-type[WT/WT]) control mice were used for the fibrotic model. Both strains of mice were injected with sequential intraperitoneal injections of fibrosis-inducing bleomycin. The mutation in the ets-2 (A72/A72) mice protected them from developing bleomycin-induced fibrosis. The ets-2 (WT/WT) mice, which did not have the mutation, were unprotected from developing fibrosis [12]. The lungs were collected at varying time points, sectioned, and imaged using multiphoton microscopy. These images were used to create the computational models in an effort to understand how to replicate the environmental forces of healthy and fibrotic lung tissue *in vitro.* This understanding will enable the development of a fibrosis-on-a-chip device with accurate mechanical properties which will provide an economical alternative to invasive and expensive clinical trials for IPF treatments and therapeutics.

2 Materials and Methods

2.1 Mice Models

Male mice containing a point mutation of ets-2 at site threonine-72 (resulting in a threonine-to-alanine conversion at site 72) were provided by medical collaborator Michael Ostrowski, Ph.D. (The Ohio State University, Columbus, OH). The mutation was generated using knockin gene targeting on an FVB/N line of mice [13,14]. The ets-2 (A72/A72) mice served as the non-fibrotic model, while WT male mice with an FVB/N background served as the fibrotic model.

2.2 Bleomycin Injections

Three ets-2 (A72/A72) mice and three ets-2 (WT/WT) mice, aged 6-12 weeks, underwent intraperitoneal injections of 0.035 U bleomycin/gram on Days 1,4,8,11,15,18,22, and 25. An additional mouse of the ets-2 (WT/WT) strain underwent injections of phosphate buffered saline (PBS) on the same days to serve as a vehicular control. Each mouse was killed on Day 11, 22, or 33 following the first injection of bleomycin and their lungs were lavaged with 1.0 ml PBS. The lungs were then harvested and inflated with 20-cm pressure, and the left lobe of each lung was placed in 10% formalin and prepared on slides for imaging [12].

2.3 Multiphoton Microscopic Imaging

Grayscale images of the prepared lung sections were taken using an Olympus FV1000 MPE Multiphoton Laser Scanning Confocal microscope provided by the Campus Microscopy & Imaging Facility at the Wexner Medical Center (The Ohio State University, Columbus, Ohio). The objective used was a 25x1.05 N.A. 2mm working distance water immersion lens. Each image had a width of 508.93 microns as well as a height of 508.93 microns. The spatial resolution of each image was 1.006 pixels per micron. The number of images taken per sample

ranged between 10 and 21 images depending on the amount of tissue variation (i.e. fibrotic vs. non-fibrotic regions) as well as the size of the tissue sample.

2.4 Image Processing

Once the microscopic images were taken, ten images from each lung were converted from grayscale images to black and white images featuring only areas of interest and background using ImageJ software. The images that were selected were the images that most accurately represented the range of tissue in that sample. First, the images were cropped to a size of 200 by 200 microns to eliminate artifacts and to ensure that the images contained only alveolar tissue and no blood vessels. The maximum threshold value of each image was then adjusted to allow the lung tissue to be completely visible while limiting the amount of background noise. This produced a black and white image consisting of black alveolar tissue boundaries and white airspaces. To eliminate any remaining background noise, the "despeckle" command was used until only the tissue boundaries and airspaces remained. The images were then saved as TIFF files.

2.5 Tissue Boundary Determination

After being processed with ImageJ, each image file was then converted into a list of between 40 and 70 domains using MATLAB (Matrix Laboratory, version R2011a) software. The script defined each airspace and freestanding piece of tissue as a domain and assigned it a number. The script then prompted the user as to whether they would like to keep or discard each boundary. This allowed for random, disconnected pieces of tissue that would interfere with the simulation results to be removed from each image. Once the user had decided which boundaries to keep or discard, the script then evaluated each domain for overlapping boundaries. If any boundary had crossed over itself, the user was provided with a graphical user interface (GUI)

where the each overlapping boundary could be assessed and fixed. The script then saved the images as text files.

2.6 Graphic Image Formatting

The text files from produced by MATLAB were then formatted for COMSOL (Multiphysics finite element analyzer, version 4.3a) software using Rhinoceros (version 3.0) software. Images were read into the Rhinoceros interface in a two dimensional plane along the x and y axes. The images were then saved as DXF (Drawing Exchange Format) files so that they could be uploaded into COMSOL.

2.7 Biaxial Tensile Test

Once the images were formatted, they were imported into COMSOL to begin simulation testing. The uploaded file served as the main geometric entity, existing as a collection of domains and tissue boundaries. The tissue boundaries were defined as an isotropic linear viscoelastic material, with a thickness of 10 microns, a Young's modulus of 5000 Pa, a Poisson's ratio of 0.48, and a density of 1000 kg/m^3 [15,16]. The entire image was then unified so that the domains would act as one unit.

In order to perform the tensile test, a buffer layer of 300 microns was added to the perimeter of the unified tissue sample. This was to dampen the edge effects of the tensile test, which originate when the tissue is pulled simultaneously in two separate directions and obscure the data [17]. The buffer layer had the same properties as the tissue. The four edges of the buffer layer were then simultaneously pulled 10 microns away from the center, resulting in a biaxial displacement in both the negative and positive x and y directions. This test was performed on each of the images, and a maximum first principal stress and strain value was calculated for each test to quantify the mechanical properties of each tissue sample. These values were obtained

from the 200 by 200 micron alveolar region of the model only; the buffer region was left out of the calculation because it was not a part of the original tissue image.

2.8 Mesh Convergence Test

In order to ensure that an appropriate number of elements were being used for the simulations, a mesh convergence test was performed using an image of lung tissue from the control mouse injected with PBS. Starting with a very coarse mesh, the biaxial tensile test was performed several times with increasingly finer mesh sizes. The maximum strain values were then graphed against the number elements in the mesh to determine an asymptotic maximum strain value for the model. This value was then used to calculate the percent error for the maximum strain value determined with each mesh size. The first mesh size that yielded an error value of less than 0.015% was used as the mesh size for the rest of the study, as it provided the most accurate measurement without utilizing unnecessary amounts of computing power.

2.9 Oscillation Test

After the stationary tests were completed, a time-dependent simulation was created to simulate the effects of breathing and examine the maximum principal stress and strain values over time. The model was set to oscillate twice per second to resemble the breathing pattern of a mouse [19] and measurements of principal stress and strain were calculated once every 0.01 seconds and graphed against time.

2.10 Statistical Testing

A paired t-test was performed to determine the significance of the changes IPF causes in the basic mechanical properties of lung tissue. The test was performed three separate times, once for Day 11-collected samples, once for Day 22 collected samples, and once for Day 33 collected samples. For each time the test was performed, the transgenic ets-2 (A72/A72) mice were paired

with the ets-2 (WT/WT) mice. Then, an ANOVA was run to determine the significance of the differences between maximum stress and strain within each genetic strain.

3 Results

3.1 Tissue Microstructure

The alveolar tissue was imaged with a multiphoton microscope, allowing very close examination of the lung tissue microstructure throughout the progression of the disease. Figure 1 shows examples of the microscopic images obtained of both genetic strains at each of the three time points. Shown in Figure 1(A) and Figure 1(B), respectively, are the ets-2 (A72/A72) and the ets-2 (WT/WT) lung tissues harvested on Day 11 after the first bleomycin injection. In Figures 1(C) and 1(D) are examples of the ets-2 (A72/A72) and the ets-2 (WT/WT) samples collected on Day 22. Figures 1(E) and 1(F) display the effects of bleomycin injection on the ets-2 (A72/A72) and the ets-2 (WT/WT) lung tissue after 33 days. In the WT strain, there is an extremely high level of scar tissue accumulation which has resulted in the shrinking of airspaces throughout the sample. The non-fibrotic strain, in comparison, remains normal with no significant tissue accumulation.

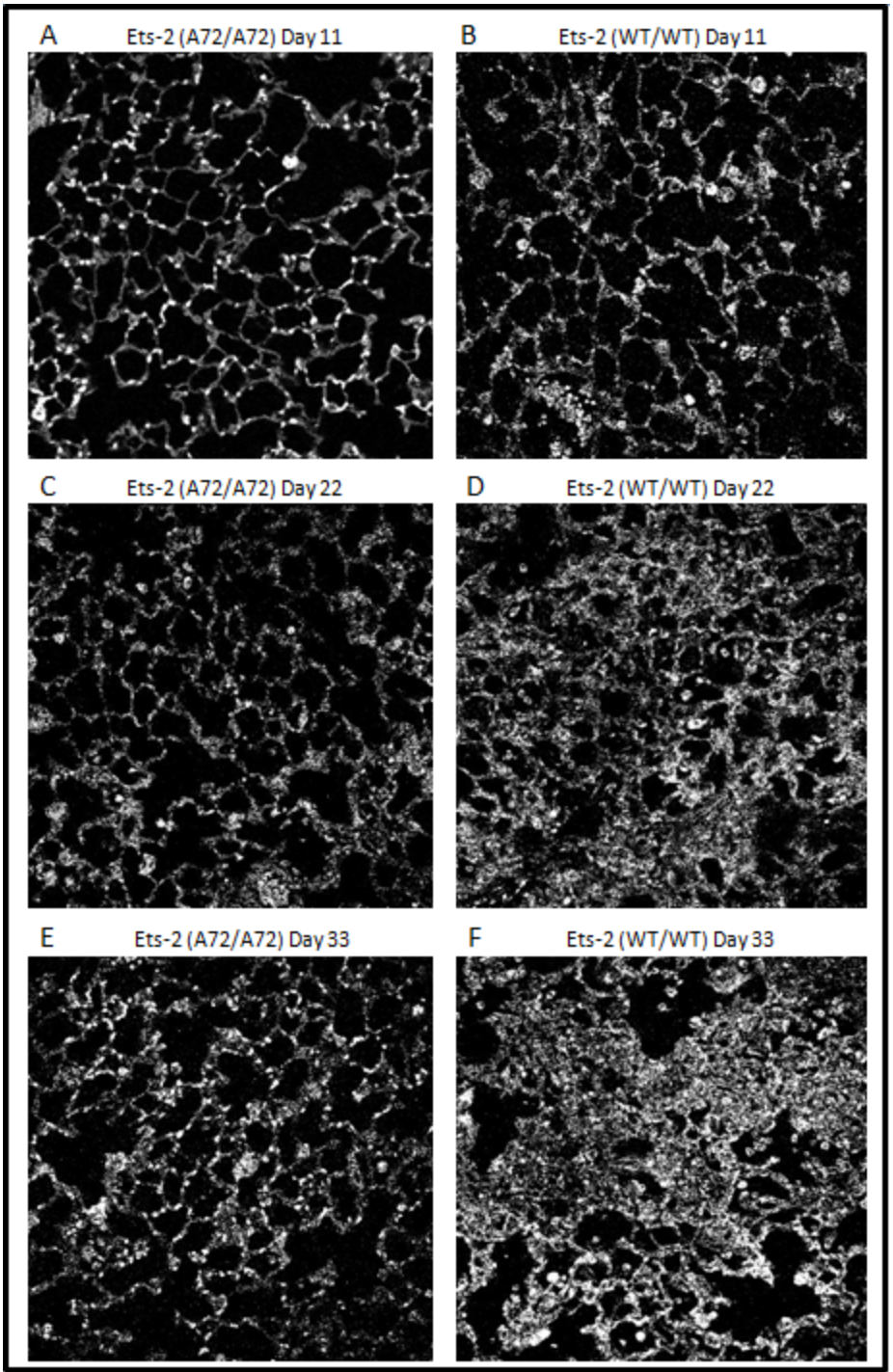

Figure 1: Pictured are images of ets-2 (A72/A72) harvested on days 11 (A), 22 (C), and 33 (E), and ets-2 (WT/WT) lung tissue harvested on days 11 (B), 22 (D), and 33 (F) taken with an Olympus FV1000 MPE Multiphoton Laser Scanning Confocal microscope.

Figure 2 displays an example of the collagen in both strains of mice at Day 33. Figure 2(A) shows the ets-2 (WT/WT) image seen in Figure 1(F) with a red pseudo color, while Figure 2(B) shows only the collagen (pseudo colored green) in the same image. Both images were taken simultaneously in two separate channels; the collagen is a second harmonic image. Figure 2(C) and 2(D), respectively, show the fibrosis-protected (A72) tissue at Day 33 (pseudo colored red) and its collagen accumulation (pseudo colored green).

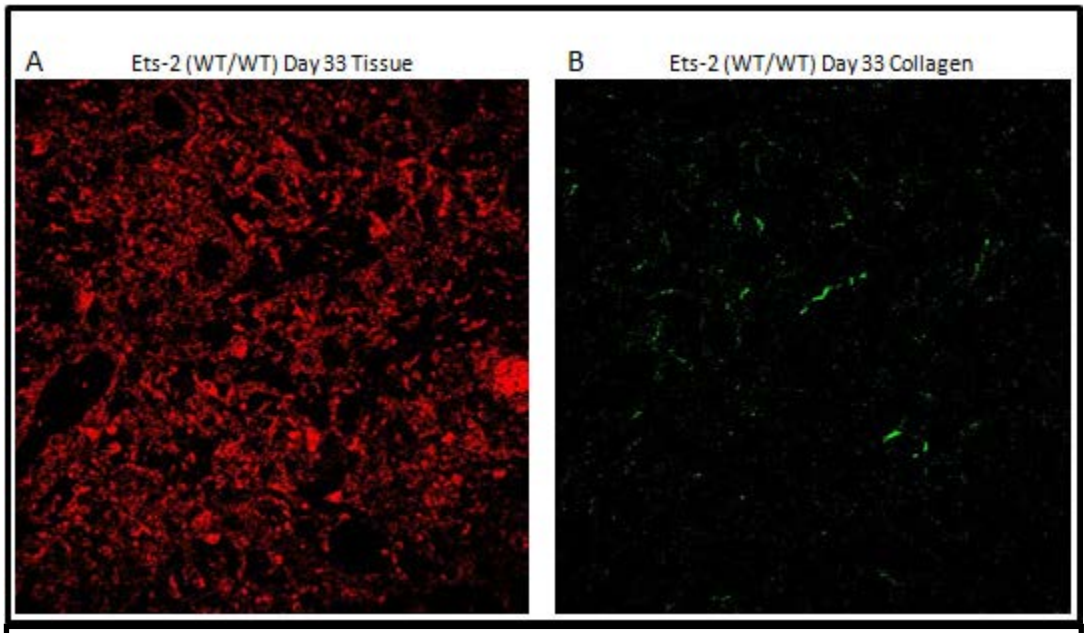

Figure 2: Image A exhibits an example of ets-2 (WT/WT) tissue collected at day 33 and pseudo colored red, while Image B exhibits only the collagen from Image A, which was image in the second harmonic and pseudo colored green.

3.2 Processed Tissue Image

After the images were processed though MATLAB, they still closely resembled the original grayscale images with respect to their tissue boundaries and alveolar spaces. Figure 3 provides a comparison of a Day 11 non-fibrotic, unprocessed microscopic image (Figure 3(A)) next to its processed black and white version after being run through the MATLAB script (Figure 3(B)).

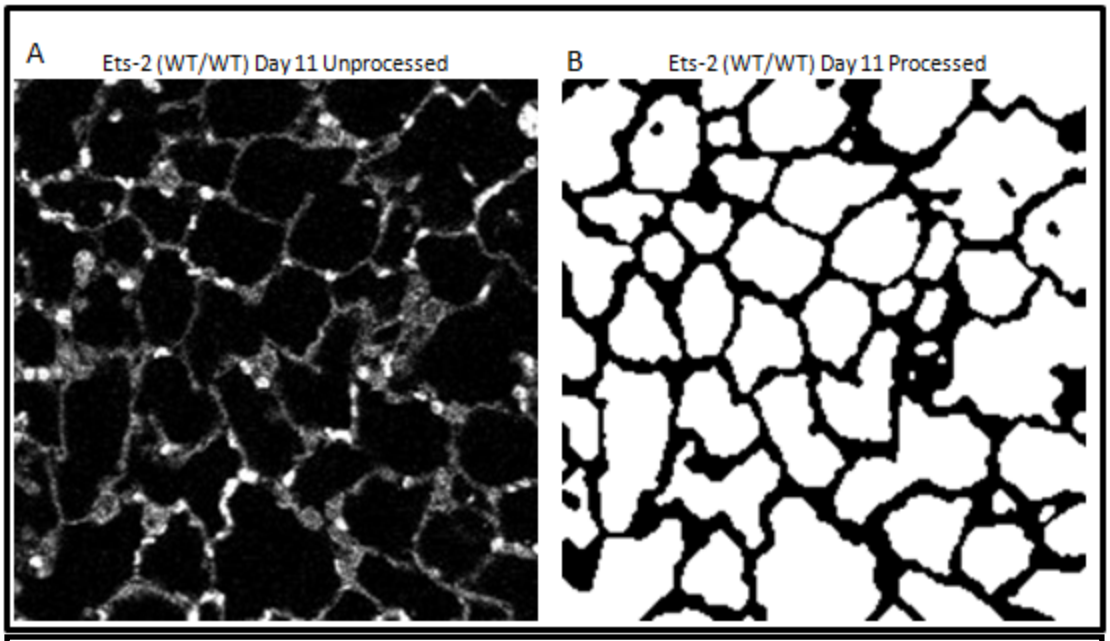

Figure 3: An unprocessed microscopic image of ets-2 (WT/WT) tissue harvested on day 11 (A) is pictured next to its processed counterpart.

3.3 Biaxial Tensile Test Analyses

After the biaxial tensile test was performed on each of the images, the maximum stress and strain values were recorded for each simulation and are shown in Table 1. The average stress and strain values for both the fibrotic and non-fibrotic tissues were calculated from these values and plotted against time. The graphs showing average stress and strain are pictured in Figures 4 and 5, respectively. When compared with the ets-2 (A72/A72) tissue, it is clear that the WT tissue is showing an upward trend in in these values as the disease progresses through Day 33. Pictured in Figure 6 are examples of the final strain plot (generated by COMSOL) for each tissue type at each time point. The color maps demonstrate strain values throughout the images, with the color range adjusted to allow the strain variation to stand out more clearly to observers.

Genetic Strain	Day of Harvest	Max. Stress (N/m^2)	Max. Strain	Genetic Strain	Day of Harvest	Max. Stress (N/m^2)	Max. Strain
ets-2(A72/A72)	11	1971.047	0.37764	ets-2(WT/WT)	11	1640.812	0.31825
ets-2(A72/A72)	11	1579.673	0.31531	ets-2(WT/WT)	11	2562.813	0.50909
ets-2(A72/A72)	11	3964.7	0.49298	ets-2(WT/WT)	11	1558.523	0.30885
ets-2(A72/A72)	11	1819.995	0.45588	ets-2(WT/WT)	11	2558.624	0.49885
ets-2(A72/A72)	11	2005.183	0.40051	ets-2(WT/WT)	11	2801.196	0.55825
ets-2(A72/A72)	11	3121.91	0.61854	ets-2(WT/WT)	11	3262.265	0.64823
ets-2(A72/A72)	11	2264.132	0.43678	ets-2(WT/WT)	11	2874.64	0.49124
ets-2(A72/A72)	11	2564.12	0.3945	ets-2(WT/WT)	11	2618.459	0.4564
ets-2(A72/A72)	22	2504.077	0.50036	ets-2(WT/WT)	22	3081.759	0.61728
ets-2(A72/A72)	22	3937.547	0.679	ets-2(WT/WT)	22	2129.061	0.42043
ets-2(A72/A72)	22	3936.671	0.38203	ets-2(WT/WT)	22	2372.567	0.47272
ets-2(A72/A72)	22	1707.287	0.33142	ets-2(WT/WT)	22	2081.759	0.61728
ets-2(A72/A72)	22	1979.222	0.38686	ets-2(WT/WT)	22	2810.309	0.56329
ets-2(A72/A72)	22	2109.945	0.41997	ets-2(WT/WT)	22	3133.86	0.62219
ets-2(A72/A72)	22	1575.34	0.44561	ets-2(WT/WT)	22	2554.48	0.64598
ets-2(A72/A72)	22	2314.194	0.41256	ets-2(WT/WT)	22	2948.56	0.61453
ets-2(A72/A72)	33	1814.578	0.36052	ets-2(WT/WT)	33	2425.736	0.48421
ets-2(A72/A72)	33	3264.26	0.65073	ets-2(WT/WT)	33	2926.42	0.52134
ets-2(A72/A72)	33	2248.822	0.44698	ets-2(WT/WT)	33	3504.216	0.6975
ets-2(A72/A72)	33	2175.276	0.43477	ets-2(WT/WT)	33	2417.216	0.49495
ets-2(A72/A72)	33	2114.658	0.4214	ets-2(WT/WT)	33	3604.249	0.71474
ets-2(A72/A72)	33	1680.665	0.39627	ets-2(WT/WT)	33	3209.175	0.63654
ets-2(A72/A72)	33	2458.941	0.49512	ets-2(WT/WT)	33	3018.469	0.69451
ets-2(A72/A72)	33	2954.156	0.34651	ets-2(WT/WT)	33	2941.645	0.73494

Table 1: Listed above are the maximum stress and strain values for the images that were run through the COMSOL simulation. The values for the ets-2 (A72/A72) mice are listed on the left, while the values for the ets-2 (WT/WT) mice are listed on the right.

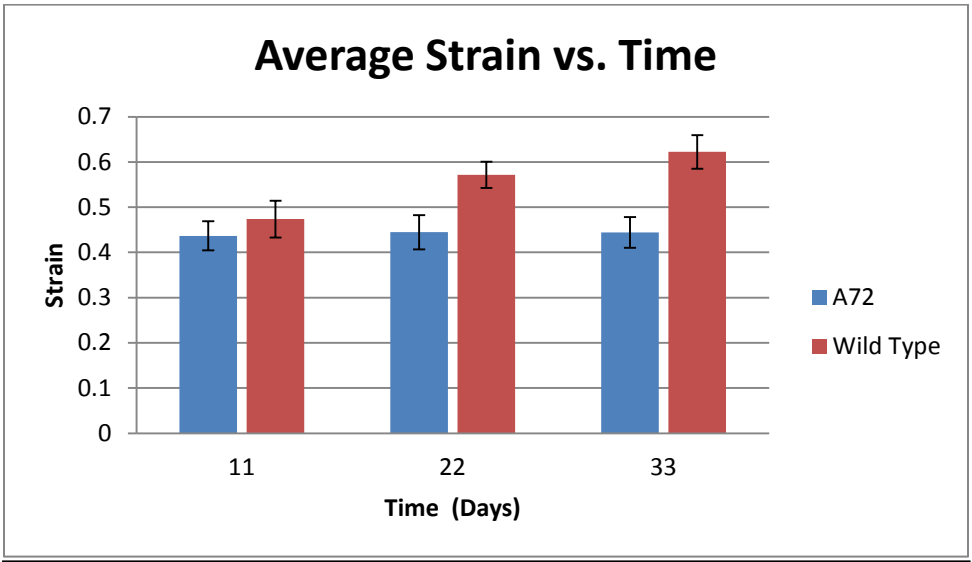

Figure 4: The averaged maximum strain values are graphed against time and shown in the image above. The ets-2 (WT/WT) tissue displays an upward trend while the mutant tissue shows little variation.

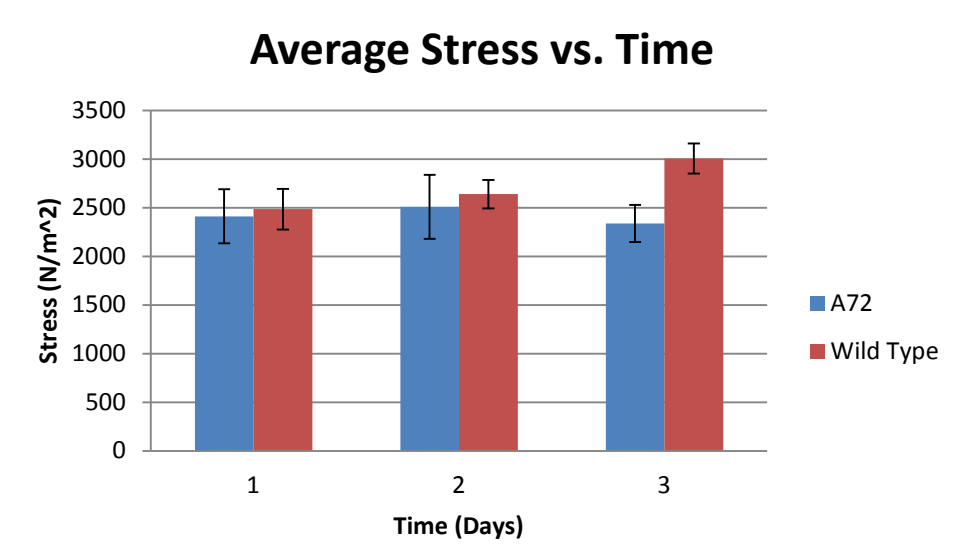

Figure 5: The averaged maximum stress values are graphed against time and shown in the image above. The ets-2 (WT/WT) tissue displays an upward as in the Figure 4, however with a proportionately larger standard error.

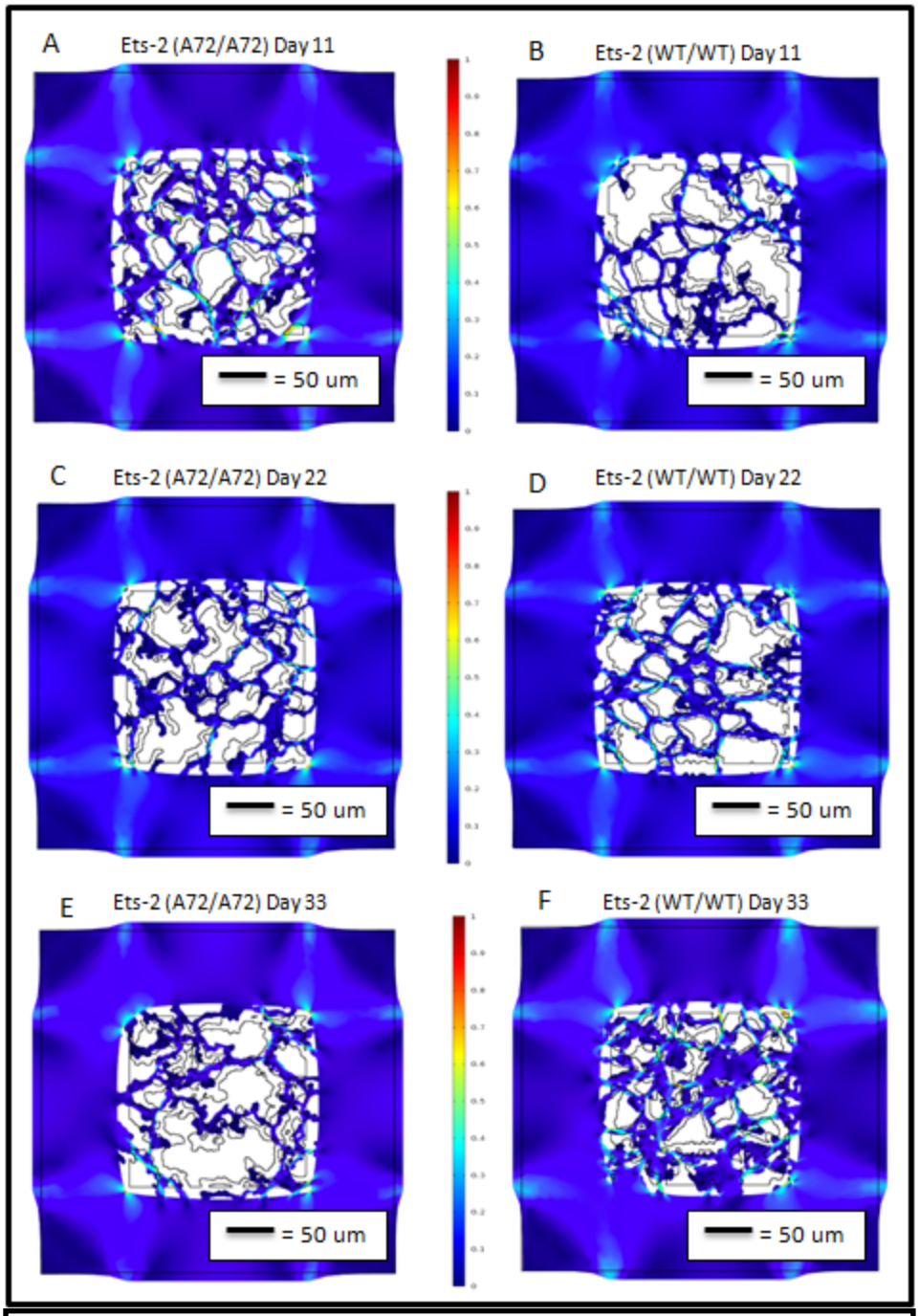

Figure 6: Pictured are images of ets-2 (A72/A72) harvested on days 11 (A), 22 (C), and 33 (E), and ets-2 (WT/WT) lung tissue harvested on days 11 (B), 22 (D), and 33 (F) after being run through the COMSOL simulation. The color map demonstrates strain relative to the maximum strain value.

3.4 Mesh Convergence

A graph displaying maximum stress vs. element number in the PBS control mouse was plotted using Excel and is pictured in Figure 7(A). This graph was used to determine the asymptotical maximum strain value the sample was approaching, which was then used to calculate percent error for each mesh size. The percent error was then plotted vs. element number and is shown in Figure 7(B). The mesh convergence test showed that the ideal mesh for the images used in this study was to have a maximum element size of 42.4 microns, a minimum element size of 0.24 microns, a maximum element growth rate of 1.3, and a curvature resolution of 0.3. An image showing a tissue sample meshed with the final element settings is shown in Figure 8(A), along with a zoomed version in Figure 8(B).

A

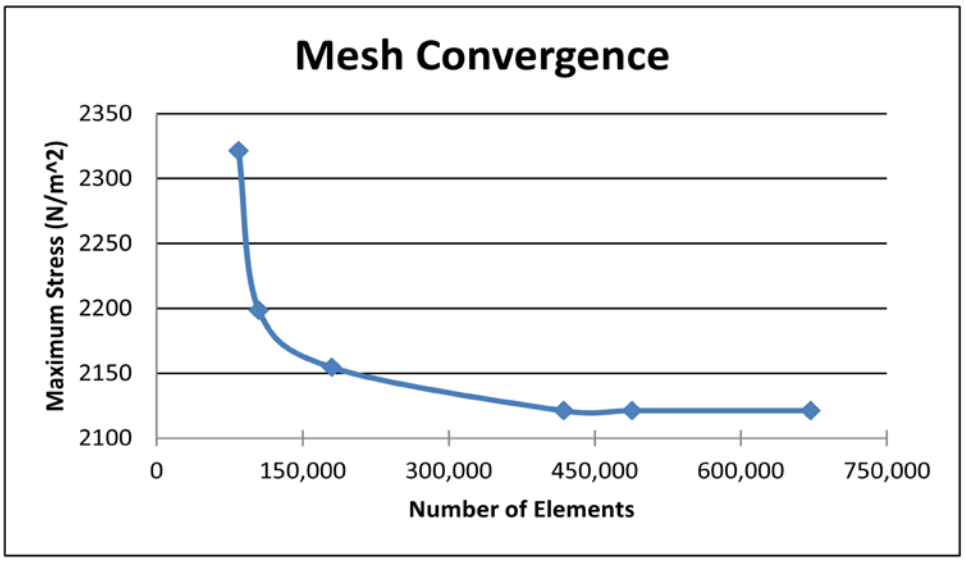

B

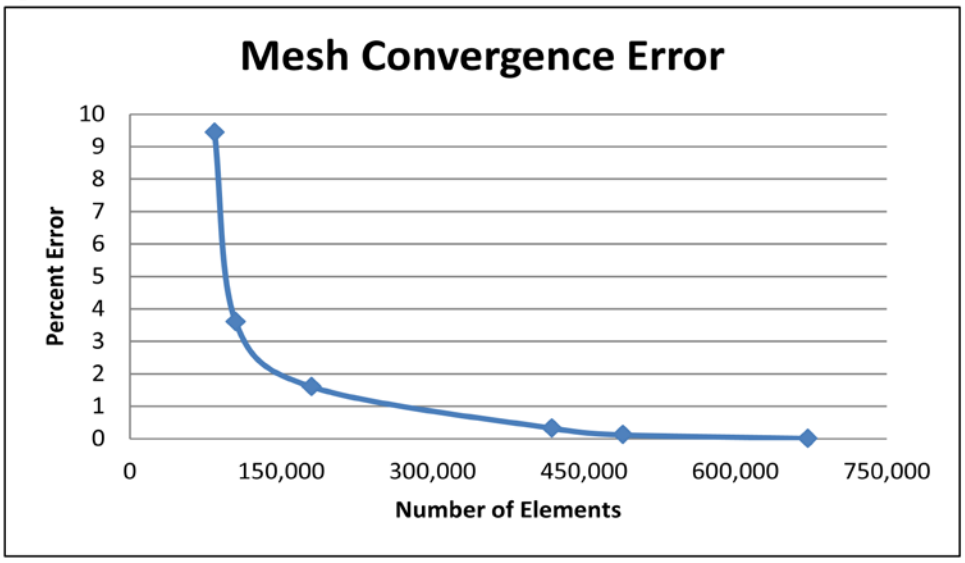

Figure 7: Image A shows a plot of mesh convergence as the number of elements in the model increases. Image B shows a plot of percent error as a function of the asymptotical value obtained from image A. This study was performed using the PBS control model.

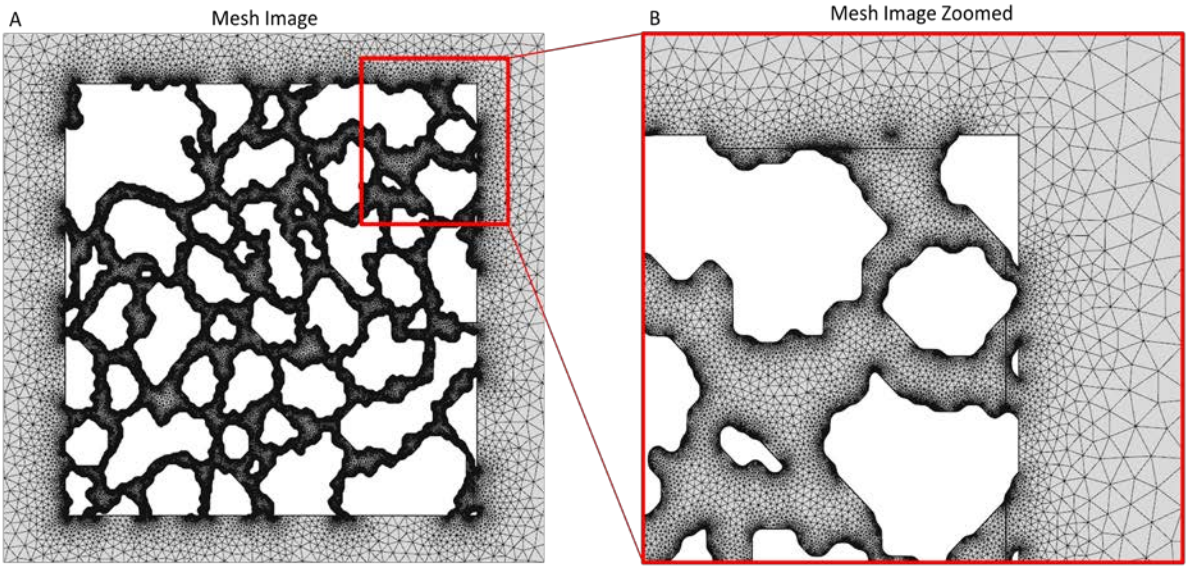

Figure 8: Shown in Image A is an ideal mesh generated with the final settings determined by the mesh convergence test. Image B is a zoomed version of the top right corner of Image A, which displays the extreme detail allowed by this element size.

3.5 Oscillation Test Analysis

After the time dependent simulation was run for two seconds of breathing time (about four breaths), graphs of stress and strain vs. time were created. The test was run on an image capture from a PBS control mouse; examples of the resulting graphs are shown in Figures 9(A) and 9(B).

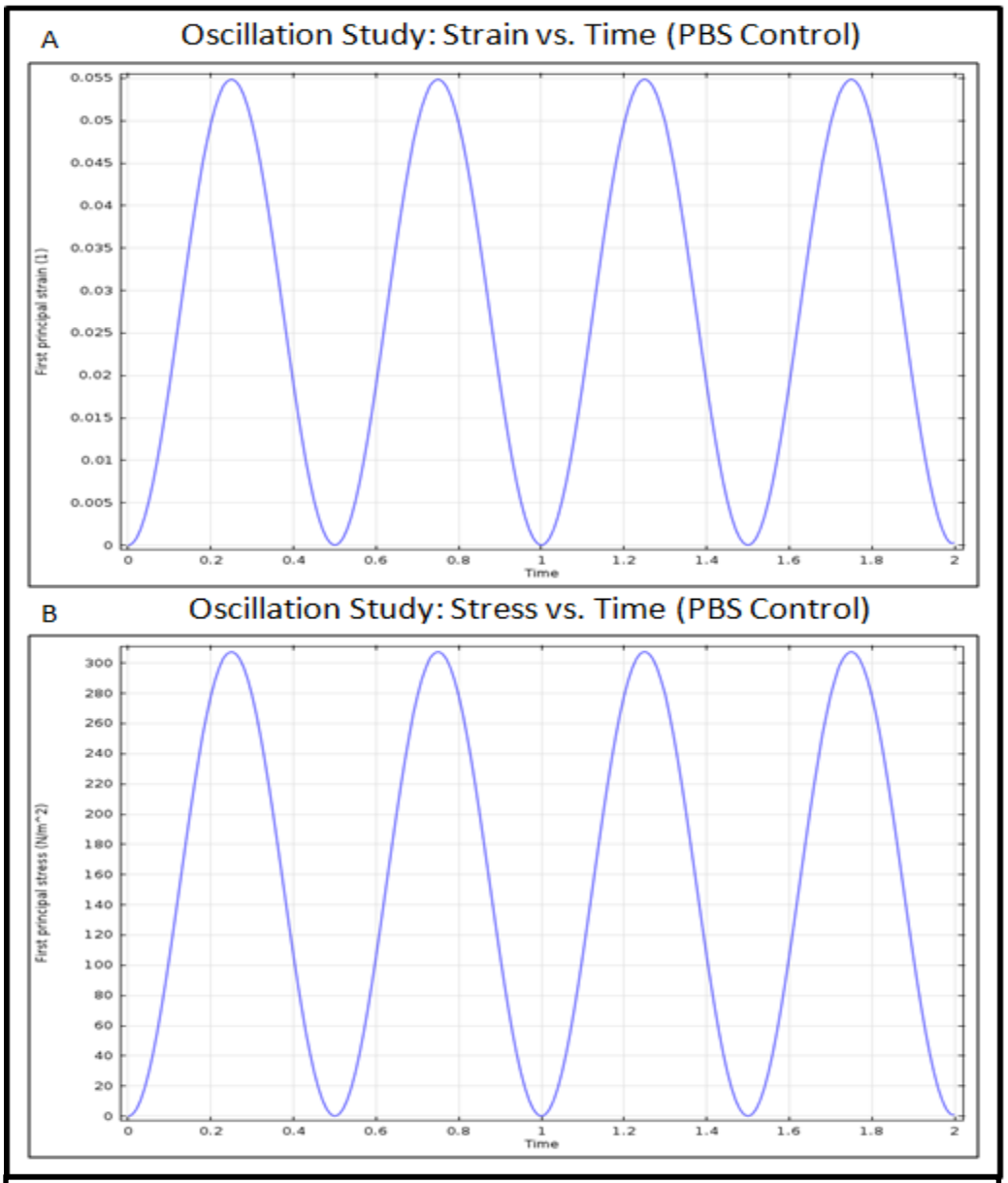

Figure 9: Pictured above are graphs of strain vs. time (A) and stress vs. time (B), using values obtained from the oscillation study. Each graph displays the equivalent of four breaths of the course of four seconds.

3.6 Statistical Analysis

The paired T-test on the differences maximum between stress and strain according to genetic strain showed that the differences in maximum strain were significant at Day 22 and Day 33, with p-values of 0.0681 and 0.01597, respectively. The maximum stress values did not become significantly different between genetic strains until Day 33, for which a p-value of 0.0309 was obtained. Figure 10 shows the one way ANOVA for maximum strain (10(A) and 10(B)) and maximum stress (10(C) and 10(D)) for the wild type mice. Figure 11 shows the one way ANOVA for maximum strain (11(A) and 11(B)) and maximum stress (11(C) and 11(D)) for the a72 transgenic mice.

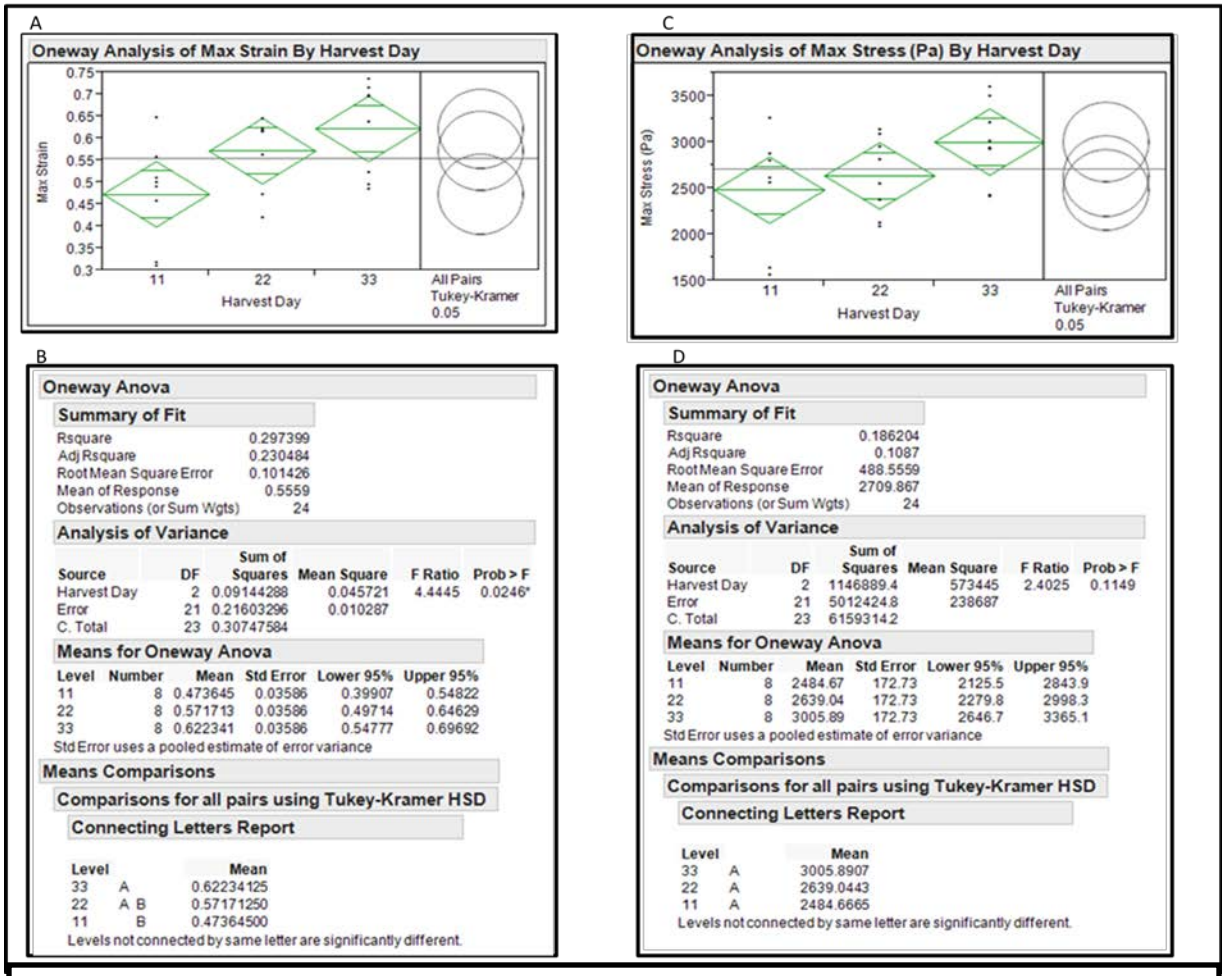

Figure 10: The data above show the one way ANOVA for maximum strain (10(A) and 10(B)) and maximum stress (10(C) and 10(D)) for the wild type mice.

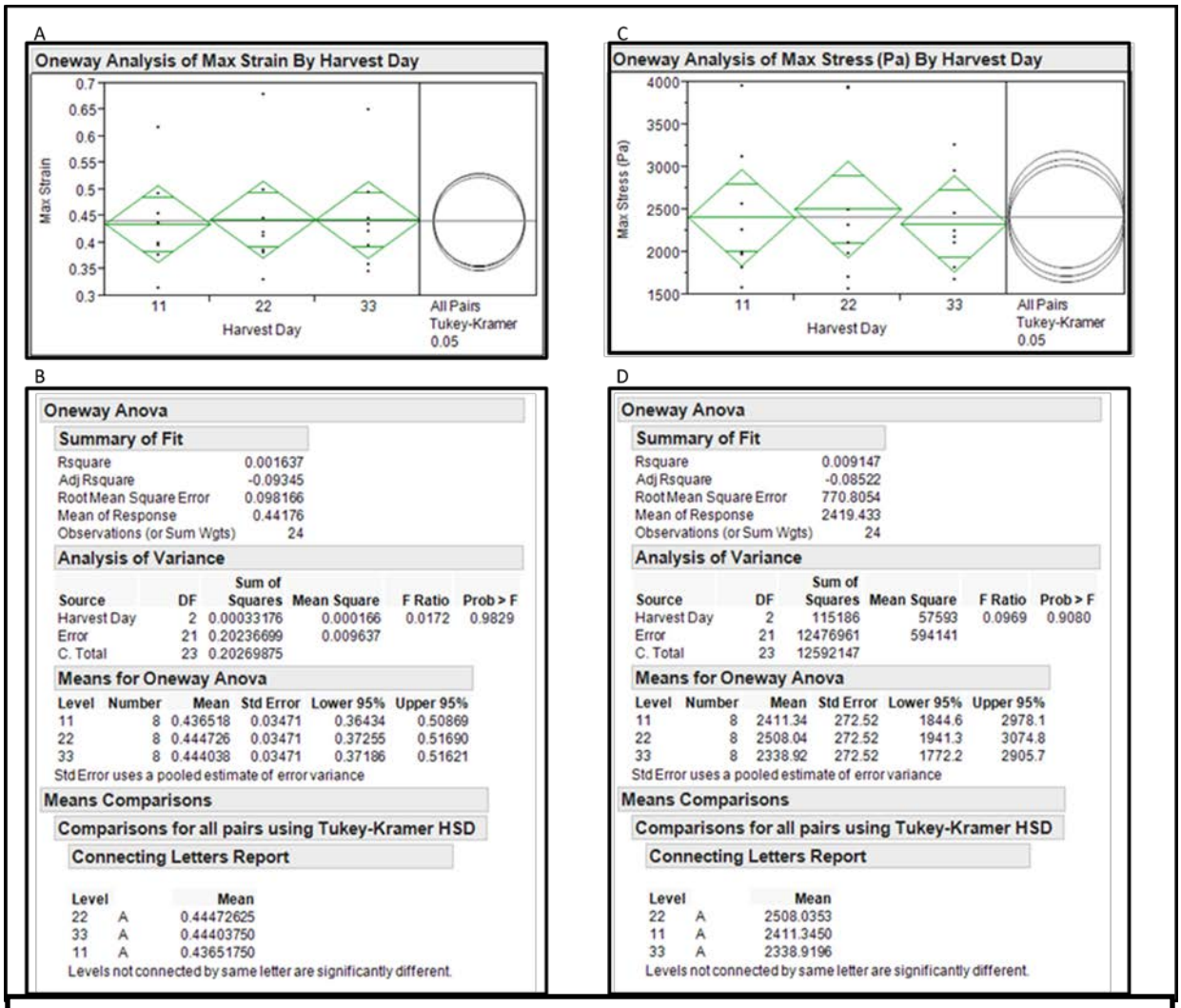

Figure 11: The data above shows the one way ANOVA for maximum strain (11(A) and 11(B)) and maximum stress (11(C) and 11(D)) for the a72 transgenic mice.

4 Discussion

4.1 Effects of Bleomycin Injection on Mouse Models

Figure 1 illustrates how the bleomycin injections affected both the ets-2 (A72/A72) and the ets-2 (WT/WT) mice over the course of 33 days. Figures 1(A), 1(C), and 1(E) demonstrate the progression of fibrosis in the transgenic mouse model. It is evident from the comparison of these images that the progression of fibrosis in these lung samples is minimal, if present at all. The alveoli maintain a characteristically hexagonal geometric shape and the alveolar walls maintain a normal thickness (about 5 microns) throughout the intraperitoneal administrations of bleomycin and several days after their completion. The cascade of reactions that occurs in a lung with IPF seems to indeed be inhibited by the A72 mutation in these mice.

The WT mice (pictured in Figures 1(B), 1(D), and 1(F) next to their transgenic counterparts), however, exhibit significant development of scar tissue as time progresses. After 11 days, the WT lung tissue has some minor scar tissue accumulation. However, many functional, large air spaces still remain at this time point. After 22 and 33 days, the WT lung tissue has a significantly larger amount of tissue accumulation in the alveolar walls. Figure 2 exemplifies that this accumulation contains collagen, a development that is characteristic of IPF [1,2]. There is evident shrinking in the diameter of the air spaces as a result of the increased scar tissue. This would have undoubtedly inhibited the breathing, mobility, and tissue oxygenation of these mice. The onset and progression of IPF is thus uninhibited and able to progress quickly in the WT strain due to the lack of an A72 transgenic mutation.

4.2 Image Processing and Graphic Formatting

The processed microscopic images, as depicted in Figure 3(B), were virtually unchanged from their original unprocessed counterparts. The only obvious dissimilarities are the conversion

from a grayscale image to a black and white reversed image, as well as a reduction in background noise. The purpose of the black and white image was to break the tissue sample down into tissue and airspaces alone, which resulted in a binary image that could be read and interpreted easily by matrix analysis software such as MATLAB. As evidenced by Figure 3, the threshold adjustment in ImageJ allowed for nearly all of the tissue to be included in the image, including the parts which were further away from the lens objective of the microscope and appeared dimmer in the grayscale image. The "despeckle" function in ImageJ proved invaluable to this process, as it allowed for the background noise caused by non-specific fluorescence speckles to be removed from the images. Had they remained in the processed images, the speckles may have impacted the reaction of the tissue samples to the biaxial tensile test.

4.3 Tissue Deformation and Mechanical Properties

Based on the results from the stationary biaxial tensile tests, the average values of maximum stress and strain at Days 11, 22 and 33 of the experiment exhibit an upward trend in the ets-2 (WT/WT) models. This mechanical change is evidenced by Figures 4 and 5. Between days 11 and 33, the WT lung tissue developed a 31% total increase in maximum strain and a 21% total increase in maximum stress. In comparison, the ets-2 (A72/A72) model did not demonstrate a significant change in maximum stress or strain values which is also evidenced by the plots in Figures 4 and 5. The static mechanical properties of the tissue remained the same due to the lack of fibrosis development.

The oscillation test was created to ensure the tissue was behaving as a linear viscoelastic material (as defined earlier in the simulation), and that oscillating the tissue was not causing its maximum stress and strain values to change over time. In both the stress and strain analyses, the maximum values remained the same after four oscillations. The model shows that the strain

values in the lung increase as it is pulled farther apart, and decrease back to the same base value as the tensile force is relaxed.

4.4 Future Testing

Although this study answered many important questions, there are several topics that still need to be investigated before final conclusions can be made about its findings. Firstly, the simulation assumes that the tissue has consistent properties throughout each sample. This is an oversimplification; the properties of lung tissue change drastically when fibrosis develops [5]. One important change is the stiffening of the tissue caused by the accumulation of irregular scar tissue. To incorporate this aspect into the model, a method will need to be developed that will allow the user to decide which tissue sections have stiffened as a result of fibrosis. One proposition would be to lay the collagen images (generated in the second harmonic) over the full tissue images, and assign the collagen domains a higher stiffness value before running the simulation in COMSOL. This could provide a better idea of the changes in lung tissue properties as IPF progresses. Additionally, other studies have striven to quantify the stiffness properties for diseased lung [21], which could be incorporated into a parameterized study to further refine the stiffness properties for the IPF model.

A second problem with the current model is that it assumes the lung tissue to be a linear viscoelastic material. However, several studies have shown that lung tissue behaves more like a nonlinear viscoelastic material [19]. If a way to accommodate this property could be integrated into the simulation, it would generate a more accurate simulation. This type of simulation may be too complicated to perform with COMSOL; additional software may need to be considered.

Additionally, the long-term purpose of the study is to define the mechanical properties of human lung tissue. However, this simulation has only been used with mouse lung tissue. Mouse

lungs are very different from human lungs, one way being that they have a different breathing frequency. The elastic and resistive properties are highly dependent on the breathing frequency of the lung [20]. Therefore, if there are to be any conclusions made about human lungs using this simulation, the tissue used will have to be human.

5 Conclusions

IPF is the most common interstitial lung disease in the world, and with a five year survival rate of 20%, is more deadly than several types of cancer. It is hypothesized to be triggered by substantial lung injury, which is then followed by a cascade of tissue accumulation as a result of the lung's inability to repair itself properly. Several studies have sought to find treatments or cures, one of which being through developing an *in vitro* model of a fibrotic lung to study lung tissue and avoid invasive clinical procedures. This study sought to improve upon the fibrosis-on-a-chip model by defining the mechanical properties of fibrotic lung tissue when it is stretched. Several different types of software including ImageJ, MATLAB, and COMSOL were utilized to develop a working simulation of a biaxial tensile test for mouse lung tissue. Several fibrotic and non-fibrotic models were run through the simulation, and it was determined that the increase in scar tissue during the development of fibrosis leads to a significant increase in maximum stress and strain values. Future steps that would be necessary for this study include incorporating varying tissue properties into the model, accommodating the natural nonlinearity of lung tissue into the model, and using the model with human lung tissue instead of mouse lung tissue. The properties quantified by this study will allow for a more accurate fibrosis-on-a-chip microdevice to be developed which will respond realistically to environmental loads, making it a cheap and reliable alternative to clinical trials in the development of IPF treatments.

Reference List

[1] TALMADGE E. KING, JR., JANET A. TOOZE, MARVIN I. SCHWARZ, KEVIN R. BROWN, and REUBEN M. CHERNIACK "Predicting Survival in Idiopathic Pulmonary Fibrosis", American Journal of Respiratory and Critical Care Medicine, Vol. 164, No. 7 (2001), pp. 1171-1181.

[2] Ganesh Raghu, Derek Weycker, John Edelsberg, Williamson Z. Bradford, and Gerry Oster "Incidence and Prevalence of Idiopathic Pulmonary Fibrosis", American Journal of Respiratory and Critical Care Medicine, Vol. 174, No. 7 (2006), pp. 810-816.

[3] Walter Nicholas, Collard HR, King Jr. TE. "Current Perspectives on the Treatment of Idiopathic Pulmonary Fibrosis", *American Journal of Respiratory and Critical Care Medicine*, Vol. 3, 2006 JUN, No. 4(2006), pp.330-338.

[4] Antoniou KM, Margaritopoulos GA, Siafakas NM. "Pharmacological treatment of idiopathic pulmonary fibrosis: from the past to the future", *European Respiratory Review*, Vol. 22 2013 SEP, No. 129, pp. 281-291.

[5] Borchers AT, Chang C, Keen CL, Gershwin ME. "Idiopathic Pulmonary Fibrosis- and Edipemiological and Pathological Review." *Clinical Reviews in Allergy & Immunology*. April 2011, Volume 40, Issue 2, pp 117-134

[6] M Eastwood, D A McGrouther and R A Brown, "Fibroblast Responses to Mechanical Forces." *Proceedings of the Institution of Mechanical Engineers, Part H: Journal of Engineering in Medicine.* 1998 212: 85.

[7] Suki B, Bates JHT. "Lung tissue mechanics as an emergent phenomenon". *Journal of Applied Physiology*. 2011;110:1111–1118.

[8] Simon BA. "Non-Invasive Imaging of Regional Lung Function using X-Ray Computed Tomography." *Journal of Clinical Monitoring and Computing.* 07-2000, Volume 16, Issue 5-6, pp 433-442

[9] Huh D., Matthews B. D., Mammoto A., et al "Reconstituting Organ-Level Lung Functions on a Chip". *Science 2010, 328, 1662–1668.*

[10] Huh D, Leslie DC, Matthews BD, Fraser JP, Jurek S, Hamilton GA, Thorneloe KS, mMcAlexander MA, and Ingber DE (2012). "A human disease model of drug toxicity-induced pulmonary edema in a lung-on-a-chip microdevice." *Sci Transl Med* 4:159ra147.

[11] Higuita-Castro N, Mihai C, Hansford DJ, Ghadiali SN. "In-Vitro Model of the Microscale Alveolar Microenvironment." *ASME*. Paper No. SBC2011-53648, pp. 359-360.

[12] Baran CP, Fischer SN, Nuovo GJ, Kabbout MN, Hitchcock CL, et al. "The transcription factor ets-2 plays an important role in the pathogenesis of pulmonary fibrosis." *Am J Respir Cell Mol Biol.* 45: 999–1006.

[13] Noda S, Asano Y, Takahashi T, Akamata K, Aozasa N, et al. . (2013) “Decreased cathepsin V expression due to Fli1 deficiency contributes to the development of dermal fibrosis and proliferative vasculopathy in systemic sclerosis.” *Rheumatology (Oxford).* [Epub ahead of print] PubMed PMID: 23287360.

[14] Nakerakanti SS, Kapanadze B, Yamasaki M, Markiewicz M, Trojanowska M (2006) “Fli1 and Ets1 have distinct roles in connective tissue growth factor/CCN2 gene regulation and induction of the profibrotic gene program.*” J Biol Chem* 281: 25259–25269.

[15] Gefen A, Elad D, Shiner RJ. “Analysis of stress distribution in the alveolar septa of normal and simulated emphysematic lungs.” *Journal of Biomechanics.* Volume 32, Issue 9, September 1999, Pages 891–897.

[16] de Ryk J, et al. "Stress distribution in a three dimensional, geometric alveolar sac under normal and emphysematous conditions". *International Journal of COPD.* 2007:2(1) 81–91.

[17] Jacobs NT et al. “Biaxial Tension of Fibrous Tissue: Using Finite Element Methods to Address Experimental Challenges Arising From Boundary Conditions and Anisotropy.” *J Biomech Eng.* Feb 2013; 135(2): 0210041-02100410.

[18] The Jackson Laboratory. “Mouse Facts.” *MouseCyc.* Web article: http://www.informatics.jax.org/mgihome/other/mouse_facts1.shtml

[19] B. Suki , A. L. Barabasi and K. Lutchen "Lung tissue viscoelasticity: Amathematical framework and its molecular basis", *J. Appl. Physiol.*, vol. 76, no. 6, pp.2749 -2759 1994.

[20] Irvin CG, bates JHT. “Measuring the lung function in the mouse: the challenge of size.” *Respir Res* 2003, 4**:**4.

[21] Liu, F., Tschumperlin, D. J. Micro-Mechanical Characterization of Lung Tissue Using Atomic Force Microscopy. *J. Vis. Exp.* (54), e2911, doi:10.3791/2911 (2011).